Interaction-Aware Decision-Making for Autonomous Vehicles in Forced Merging Scenario Leveraging Social Psychology Factors

Xiao Li*, Kaiwen Liu*, H. Eric Tseng[†], Anouck Girard*, Ilya Kolmanovsky*

Abstract—Understanding the intention of vehicles in the surrounding traffic is crucial for an autonomous vehicle to successfully accomplish its driving tasks in complex traffic scenarios such as highway forced merging. In this paper, we consider a behavioral model that incorporates both social behaviors and personal objectives of the interacting drivers. Leveraging this model, we develop a receding-horizon control-based decision-making strategy, that estimates online the other drivers' intentions using Bayesian filtering and incorporates predictions of nearby vehicles' behaviors under uncertain intentions. The effectiveness of the proposed decision-making strategy is demonstrated and evaluated based on simulation studies in comparison with a game theoretic controller and a real-world traffic dataset.

I. Introduction

One of the major challenges in autonomous driving lies in ensuring safe interaction with nearby traffic, particularly in highway merging scenarios. Unlike the simple stop-and-go strategy used in urban intersections with stop signs, the onramp ego vehicle must cooperate with high-speed vehicles and transition itself into the highway traffic in a secure, but also timely manner. Moreover, the varied social behaviors of different drivers can result in diverse responses to the merging intent. In this dynamic interaction, the ego vehicle must actively search for available space or create opportunities for merging. A cooperative driver on the highway may decelerate or change lanes to facilitate the merging process, while a selfinterested driver may maintain a constant speed and disregard the merging vehicle. Consequently, understanding the driving intentions of the surrounding vehicles becomes crucial for the ego vehicle to accomplish its task successfully.

Learning-based methods have been extensively explored for autonomous driving applications. Without explicit interaction behavior modeling, Reinforcement-Learning (RL) based methods have been utilized to learn end-to-end driving policies [1]. Additionally, researchers have employed imitation learning to train decision-making modules that emulate expert behavior, such as a Model Predictive Controller [2]. A comprehensive survey of RL methods in autonomous driving research can be found in [3]. However, a significant drawback of end-to-end RL-learned policies is the lack of

interpretability; furthermore, their ability to generalize may be limited by the interaction observed in the training data.

To address this challenge, researchers have explored the integration of learning-based methods with planning and control techniques. The Inverse Reinforcement Learning (IRL) approach has been employed to learn the reward function of human drivers for planning purposes [4], [5]. Additionally, neural network models, such as the Social Generative Adversarial Network [6], have been implemented in trajectory prediction modules for Model Predictive Control (MPC) [7]. Novel network architectures have also been designed to enhance driving motion forecasting [8], [9]. However, a common issue in these learned modules is their limited generalization capability beyond the training dataset.

Game theoretic approaches have also been considered to represent interactions between agents in traffic, such as the Level-k method [10], and Stackleberg games [11]. A Leader-Follower Game theoretic Controller (LFGC) has been proposed specifically for modeling pairwise leader-follower interactions in forced merging scenarios in [12]. Inspired by the concepts in [12], we adopt a pairwise interaction formulation to model vehicle cooperative behaviors, enabling better scalability for scenarios involving multiple vehicles.

Differently from [12], to create a more comprehensive model of human driving, we design a novel behavioral model that incorporates various social psychology factors. Early studies in social psychology have revealed that individuals don't always act solely to maximize their own rewards in experimental games [13]. Drawing inspiration from the concept of Social Value Orientation (SVO) [13], [14], and its application in autonomous driving [15], we propose a novel behavioral model that encompasses both the drivers' inclination towards social cooperation and their individual objectives as latent parameters. Leveraging this behavioral model, we can estimate the underlying driving intentions of the interacting vehicles and make appropriate decisions for the ego vehicle in forced merging scenarios. The algorithms we propose offer several potential advantages:

- 1) The behavioral model incorporates aspects of both the driver's social cooperativeness and personal objectives and captures a rich and realistic set of behaviors.
- The algorithm uses a Bayesian filter to infer the latent driving intent parameters, thereby handling uncertainties in the cooperation intent of interacting vehicles.
- 3) The decision-making module adopts a pairwise interaction formulation and utilizes receding-horizon optimization-based control, leading to good scalability while ensuring safety for forced merging applications.

^{*}Xiao Li, Kaiwen Liu, Anouck Girard, and Ilya Kolmanovsky are with the Department of Aerospace Engineering, University of Michigan, Ann Arbor, MI 48109, USA. {hsiaoli, kwliu, anouck, ilya}@umich.edu

[†]H. Eric Tseng Retired Senior Technical Leader, Ford Research and Advanced Engineering, Chief Technologist, Excelled Tracer LLC. hongtei.tseng@gmail.com

This research was supported by the University of Michigan / Ford Motor Company Alliance program, and by the National Science Foundation under Awards CMMI-1904394 and ECCS-1931738.

This paper is organized as follows: In Sec. II, we introduce the problem setting and the forced merging scenario. We also outline the assumptions made regarding vehicle kinematics, action space, and driver's action objectives. In Sec. III, we present our behavioral model that incorporates the cooperation intents and personal objectives of the interacting vehicles. In Sec. IV, we present the decision-making module for the ego vehicle, that effectively handles uncertainties in the driving intentions of the interacting vehicles. In Sec. V, we demonstrate the ability of our behavioral model to reproduce realistic driving behaviors. Furthermore, we validate the proposed controller through simulations in comparison with the LFGC and real-world dataset evaluations. Finally, the conclusions are given in Sec. VI.

II. PROBLEM FORMULATION

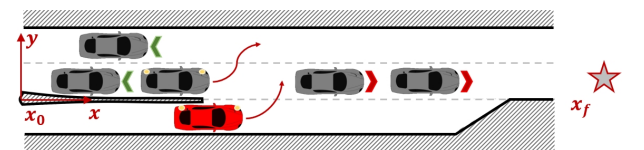


Fig. 1: Schematic diagram of the highway forced merging problem: an ego vehicle (red) interacts with highway vehicles (grey) to facilitate its merging.

In this paper, we focus on the design of a decision-making module for autonomous driving applications in forced merging scenarios. The decision-making module plans highlevel behaviors such as acceleration, deceleration, or lane changing, and generates desired reference trajectories for the autonomous vehicle. Subsequently, a lower-level controller is assumed to be available that can control the steering and acceleration/braking of the vehicle to track the reference trajectory. As illustrated in Fig. 1, the goal is to design a behavior planner for the ego vehicle to merge into the target highway lane while accounting for interactions with multiple highway vehicles to ensure safe and effective merging.

A. Vehicle Kinematics Model

We use the following discrete-time model to represent the vehicle kinematics,

$$\begin{bmatrix} x(t+1) \\ v_x(t+1) \\ y(t+1) \end{bmatrix} = \begin{bmatrix} x(t) + v_x(t)\Delta t \\ v_x(t) + a(t)\Delta t \\ y(t) + v_y(t)\Delta t \end{bmatrix} + \tilde{w}(t), \quad (1)$$

where x, v_x , and a are the longitudinal position, velocity, and acceleration, respectively; y and v_y are the lateral position and velocity; $\Delta t > 0$ is the sampling period between discrete time instances t and t+1; $\tilde{w}(t) \in \mathbb{R}^3$ is a disturbance representing unmodeled dynamics.

We assume all the vehicles, including both ego and highway vehicles, follow this dynamics model. For simplicity, Eq. (1) can be rewritten as,

$$s_i(t+1) = f(s_i(t), u_i(t)) + \tilde{w}_i(t), i = 0, 1, 2, \dots,$$
 (2)

where $s_i(t) = [x(t), y(t), v_x(t)]^T$ and $u_i(t) = [a(t), v_y(t)]^T$ represent the state and control of the *i*-th vehicle at time instance t, respectively. In the following context, the subscript i=0 designates the ego vehicle, while $i\in\{1,2,\ldots\}$ represents another vehicle with which the ego vehicle interacts.

B. Action Space

We assume vehicles take actions from the action set ${\cal U}$ that comprises:

- 1) "Maintain": keep the current lateral position and longitudinal speed;
- 2) "Accelerate": keep the current lateral position and accelerate at $a \, \text{m/s}^2$ without exceeding the upper speed limit $v_{\text{max}} \, \text{m/s}$;
- 3) "Decelerate": keep the current lateral position and decelerate at -a m/s² without falling below the lower speed limit v_{\min} m/s;
- 4) "Steer to the left": keep the current longitudinal speed and steer to the left adjacent lane with a constant lateral velocity of ^{w_{lane}}/_{T_{lane}} m/s;
 5) "Steer to the right": keep the current longitudinal speed
- 5) "Steer to the right": keep the current longitudinal speed and steer to the right adjacent lane with a constant lateral velocity of $-\frac{w_{lane}}{T_{lane}}$ m/s.

Note that we assume a complete lane change takes $T_{\rm lane}$ sec to move into the adjacent lane with a lateral traveling distance of lane width $w_{\rm lane}$, which is reflected by the above actions. We also note that more acceleration and deceleration levels |a| can be introduced to the action space, but we only consider one level here for simplicity.

C. Driving Objectives

The driving objectives of each vehicle are reflected in the reward function that depends on the following four variables:

- 1) Traffic rules c: The binary variable $c \in \{0,1\}$ is an indicator for either getting into a collision with other vehicles or getting beyond the road boundaries. A safety bounding box is constructed that overbounds each vehicle body in the x-y plane with certain safety margins. The value of c=1 indicates the overlap of two vehicles' bounding boxes or the overlap between the vehicle's bounding box and the road boundary. The value of c=0 indicates that the vehicle stays within the road and is not in collision with other vehicles. The visualization of the highway road boundaries is shown in Fig. 1 using solid black lines.
- 2) Safety consciousness h: The variable $h \in [0,1]$ is derived from the Time-to-Collision (TTC) with a vehicle ahead in the same lane (assume constant speed)

$$h = \frac{\operatorname{sat}_{[T_{\min}, T_{\max}]}(TTC) - T_{\min}}{T_{\max} - T_{\min}},$$

where $T_{\min}=0.2$ sec is the minimum reaction time, $T_{\max}=3$ sec stands for an adequate time headway, and $\operatorname{sat}_{[a,b]}(\cdot)$ is a saturation function between the minima a and the maxima b. The reward function depends on b to encourage vehicles to keep an appropriate headway distance and be conscious of potential collisions.

3) Traveling time τ : The variable $\tau \in [0, 1]$ reflects the objective of shortening the traveling time, and is a weighted summation of

$$\tau_{x} = \frac{x - x_{0}}{x_{f} - x_{0}}, \tau_{y} = 1 - \frac{1}{w_{\text{lane}}} \min \left(\left| y - y_{r} \right|, w_{\text{lane}} \right),$$

where x_0 and x_f (see Fig. 1) are the x-coordinates of the beginning of the ramp and a goal placed a specified distance away from the end of the ramp, respectively, while y_r corresponds to the center of the highway lane that is next to the ramp. The reward for τ_x promotes the highway vehicle reaching the end of the highway in a shorter time. A higher reward for τ_y is imposed for on-ramp vehicles to encourage merging action.

4) Control effort e: The reward for $e \in [0,1]$ promotes vehicles to drive at a constant speed and to reduce acceleration/deceleration. The variable e attains a value of 1 under the action "maintain"; its value decreases if the vehicle makes speed changes or lane changes.

III. SOCIAL BEHAVIOR MODELING

In this section, we introduce our behavioral model that captures drivers' interactive decision-making process during the forced merge scenario. Inspired by social psychology studies [13], [14], and its application in the context of autonomous driving [15], we define the SVO-based reward model in Sec. III-A. In Sec. III-B, we integrate this reward model into the interacting vehicle's decision-making process.

A. Social Value Orientation and Multi-modal Reward

We assume each vehicle i interacts pairwise with each adjacent vehicle $j \in A(i)$, where A(i) contains indices of all nearby vehicles in the same lane or adjacent lanes as vehicle i. We assume each driver aims to achieve their personal objectives and, to a certain extent, is cooperating with others. Hence, we model each driver's intention using a multi-modal reward function of the form

$$R_{i}(s(t), u(t)|\sigma_{i}, w_{i}) = \frac{1}{|A(i)|} \sum_{j \in A(i)} \cdot \left[\theta_{1}(\sigma_{i}) \cdot r_{i}(s_{i}(t), u_{i}(t), s_{j}(t), u_{j}(t)|w_{i}) + \theta_{2}(\sigma_{i}) \cdot r_{j}(s_{j}(t), u_{j}(t), s_{i}(t), u_{i}(t)|w_{j}) \right],$$

$$(3)$$

where $u(t) = [u_i^T(t), u_{A(i)}^T(t)]^T$ is the aggregated control vector of all vehicles and $u_{A(i)}(t)$ is a column vector concatenating $u_j(t)$ for all $j \in A(i)$; $s(t) = [s_i^T(t), s_{A(i)}^T(t)]^T$ reflects the state of the traffic at time t; |A(i)| is the number of interacting vehicles; $r_i(\cdot)$ and weights $w_i \in \mathbb{R}^3$ model personal reward as a weighted summation of personal objectives defined in Sec. II-C,

$$r_i(s_i, u_i, s_i, u_i | w_i) = (\neg c) \cdot w_i^T \cdot [h, \tau, e]^T. \tag{4}$$

The symbol \neg in Eq. (4) is the logical negation operator and σ_i in Eq. (3) takes one of four values corresponding to four SVO categories and specifies values of $\theta_1(\sigma_i)$ and $\theta_2(\sigma_i)$:

$$(\theta_1, \theta_2) = \begin{cases} (0, 1) & \text{if } \sigma_i = \text{altruistic,} \\ (1/2, 1/2) & \text{if } \sigma_i = \text{prosocial,} \\ (1, 0) & \text{if } \sigma_i = \text{egoistic,} \\ (1/2, -1/2) & \text{if } \sigma_i = \text{competitive.} \end{cases}$$
(5)

Note that in Eq. (3), θ_1 and θ_2 correspond to the weight of the self-reward r_i and the weight of the other drivers' net reward, respectively.

In this multi-modal reward given by Eq. (3), there are two latent parameters (σ_i, w_i) that represent different driving incentives: w_i reflects different personal goals, and σ_i represents different social behaviors or levels of cooperativeness. For instance, a driver with weights $w_i = [0, 1, 0]^T$ in Eq. (4) might consider driving at full speed thereby minimizing the traveling time. As implied by Eq. (3), a "prosocial" driver has equal weights for personal objectives and other drivers' objectives; hence such drivers intend to cooperate with others in pursuing a large net reward. Note that w_i is the internal parameter of vehicle j and is a latent variable affecting the decision of vehicle i if $\sigma_i \neq$ "egoistic" and $j \in A(i)$. Nonetheless, an altruistic or prosocial (or competitive) driver of vehicle i is likely to improve (or diminish) other drivers' rewards in all three variables if they do not know other drivers' objectives w_i a priori. Therefore, we assume that during the *i*-th vehicle's decision-making, $w_i = [1/3, 1/3, 1/3]$ in Eq. (3) for $j \in A(i)$.

B. Driving Behavior Model

In our behavior model, we assume the driver of vehicle i aims to maximize the cumulative reward, defined as

$$Q_i'(s(t), \gamma_i | \sigma_i, w_i) = \mathbb{E}_{\gamma_j, j \in A(i)} \left[\sum_{k=0}^{N-1} \lambda^k R_i(s(t+k), u(t+k) | \sigma_i, w_i) \right],$$
 (6)

where $\gamma_i = \{u_i(t+k)\}_{k=0}^{N-1} \in U^N \text{ is an action sequence over a horizon of length } N, \text{ and } \lambda \in [0,1] \text{ is a discount factor. This cumulative reward is an averaged reward over all possible action sequences } \gamma_j \text{ of vehicles } j \in A(i), \text{ assuming a uniform distribution. Furthermore, the driver of vehicle } is assumed to adopt a receding horizon control strategy, i.e.,$

$$u_i^*(t) = \underset{u \in U}{\operatorname{argmax}} Q_i(s(t), u | \sigma_i, w_i), \tag{7}$$

where $Q_i(s(t),u) = \mathbb{E}_{\gamma_i \in \Gamma^1(u)} \left[Q_i'(s(t),\gamma_i | \sigma_i,w_i) \right]$ and $\Gamma^1(u) = \left\{ \gamma_i = \{u_i(t+k)\}_{k=0}^{N-1} : u_i(t) = u \right\}$ contains all the action sequences with the initial action u. Furthermore, considering stochasticity in the decision-making process, a policy distribution can be prescribed by adopting a softmax decision rule [16]:

$$\mathbb{P}(u_i = u | \sigma_i, w_i, s(t)) \propto \exp\left(Q_i(s(t), u | \sigma_i, w_i)\right). \tag{8}$$

Based on the behavioral model defined above, the model parameters σ_i, w_i can affect action policies to represent different driving intentions. Since other drivers' intentions are not known in a given traffic scenario, the model parameters σ_i, w_i (i.e., drivers' intentions) need to be estimated and updated online so that the autonomous ego vehicle is able to make optimal merging decisions.

IV. DECISION-MAKING UNDER COOPERATION INTENT UNCERTAINTY

We now develop a decision-making algorithm to facilitate the forced merging process. We first present a Bayesian filter for the ego vehicle that estimates the latent variables σ_i, w_i of the interacting vehicles online. Considering the uncertainties in estimation of other drivers' intentions, we use a receding-horizon control formulation to simultaneously address the safety and performance aspects of the forced merging.

A. Bayesian Inference of Latent Driving Intentions

At each time step, we assume that the ego vehicle can observe the traffic nearby the *i*-th interacting vehicle where $i \in A(0)$, and the observed traffic history is defined as

$$\xi(t) = \{s(0), s(1), \dots, s(t), u_{A(i)}(0), u_{A(i)}(1), \dots, u_{A(i)}(t-1)\},\$$

where $s(t) = [s_i^T(t), s_{A(i)}^T(t)]^T$ and $u_{A(i)}(t)$ is a column vector concatenating $u_j(t)$ for all $j \in A(i)$. The ego vehicle utilizes the traffic history to estimate the posterior distribution $\mathbb{P}\left(\sigma_i, w_i | \xi(t+1)\right)$ of the i'th interacting vehicle's latent parameters using the following proposition:

Proposition 1. Given a prior $\mathbb{P}(\sigma_i, w_i | \xi(t))$ and assuming that the disturbance $\tilde{w}_i(t) \sim \mathcal{N}(0, Q)$ is zero-mean Gaussian, and the interacting drivers follow policy according to Eq. (8), the posterior distribution can be computed as

$$\mathbb{P}\left(\sigma_{i}, w_{i} | \xi(t+1)\right) = \frac{\Lambda_{i}\left(\sigma_{i}, w_{i}, s(t), s_{i}\right)}{N_{i}(t)} \cdot \mathbb{P}\left(\sigma_{i}, w_{i} | \xi(t)\right),$$
(9)

where $N_i(t)$ is a normalization factor and $\Lambda_i(\sigma_i, w_i, s(t), s_i)$ admits the following form:

$$\Lambda_{i}\left(\sigma_{i}, w_{i}, s(t), s_{i}\right) = \sum_{u \in U} \mathbb{P}\left(u_{i} = u | \sigma_{i}, w_{i}, s(t)\right) \cdot \\
\mathbb{P}\left(\tilde{w}_{i}(t) = s_{i} - f(s_{i}(t), u)\right),$$
(10)

where $\mathbb{P}(u_i = u | \sigma_i, w_i, s(t))$ is defined in Eq. (8).

Note that the above recursive Bayesian filter can be initialized using a uniform distribution and the covariance matrix Q is a tunable parameter. Intuitively, if we consider the current traffic state s(t) and the vehicle i is executing policy defined in Eq. (8) conditioned on parameters σ_i and w_i , Λ_i (σ_i , w_i , s(t), s_i) represents the transition probability of the vehicle i moving from $s_i(t)$ to $s_i(t+1) = s_i$. The proof is presented as follows:

Proof. Applying the Bayesian rule, the posterior admits the following form,

$$\begin{split} & \mathbb{P}\left(\sigma_i, w_i | \xi(t+1)\right) = \mathbb{P}\left(\sigma_i, w_i | s(t+1), u_{A(i)}(t), \xi(t)\right) \\ & = \frac{\mathbb{P}\left(s(t+1) | \sigma_i, w_i, u_{A(i)}(t), \xi(t)\right)}{\mathbb{P}\left(s(t+1) | u_{A(i)}(t), \xi(t)\right)} \cdot \mathbb{P}\left(\sigma_i, w_i | \xi(t)\right). \end{split}$$

Moreover, the likelihood $\mathbb{P}\left(s(t+1)|\sigma_i,w_i,u_{A(i)}(t),\xi(t)\right)$ can be decomposed to $\mathbb{P}\left(s_{A(i)}(t+1)|u_{A(i)}(t),s_{A(i)}(t)\right)$ $\mathbb{P}\left(s_i(t+1)|\sigma_i,w_i,s(t)\right)$, whereby the posterior reduces to

$$\mathbb{P}\left(\sigma_{i}, w_{i} | \xi(t+1)\right) \propto \\ \mathbb{P}\left(s_{i}(t+1) | \sigma_{i}, w_{i}, s(t)\right) \cdot \mathbb{P}\left(\sigma_{i}, w_{i} | \xi(t)\right),$$

and $\Lambda_i(\sigma_i, w_i, s(t), s_i) = \mathbb{P}(s_i(t+1)|\sigma_i, w_i, s(t))$ is the transition probability conditioned on the model parameters σ_i , w_i and the current traffic state s(t).

B. Receding-horizon Optimization-based Control

We leverage the receding horizon control to achieve safe merging. The objective of successful merging without collisions can be translated into maximizing predictive cumulative reward,

$$Q_0'(s(t), \gamma_0) = \frac{1}{|A(0)|} \sum_{i \in A(0)} \mathbb{E} \\ \left\{ \mathbb{E} \\ \gamma_i \sim \mathbb{P}(\gamma_i | \sigma_i, w_i, s(t))} \left[\overline{Q}_0' \left(s_0(t), s_i(t), \gamma_0, \gamma_i \right) \right] \right\},$$

$$(11)$$

where A(0) contains indices of all the vehicles near the ego vehicle; γ_0, γ_i are action sequences of length N corresponding to the ego vehicle and the vehicle i; $\mathbb{P}\left(\sigma_i, w_i | \xi(t)\right)$ is the posterior distribution of the latent parameted by the Bayesian filter; similar to Eq. (8), $\mathbb{P}\left(\gamma_i | \sigma_i, w_i, s(t)\right)$ is an augmented policy distribution derived from Eq. (6) such that $\mathbb{P}\left(\gamma_i | \sigma_i, w_i, s(t)\right) \propto \exp\left(Q_i'(s(t), \gamma_i | \sigma_i, w_i)\right)$; $\overline{Q}_0'(\cdot)$ computes the discounted cumulative reward of the ego vehicle according to $\overline{Q}_0'(s_0(t), s_i(t), \gamma_0, \gamma_i) = \sum_{k=0}^{N-1} \lambda^k r_0(s_0(t+k), u_0(t+k), s_i(t+k), u_i(t+k))$ and the one-step reward function $r_0(s_0, u_0, s_i, u_i) = (\neg c) \cdot \tau$ encourages collision avoidance and faster merging. Note that we can also customize r_0 for other implementation requirements, e.g., add variable τ of other drivers to r_0 to mitigate traffic congestion introduced by the ego vehicle's merging action.

Here, we model the ego vehicle interactions pairwise with the nearby vehicles $i \in A(0)$. For each interaction vehicle i, the outer expectation in Eq. (11) considers all possible combinations of parameters σ_i, w_i that illustrate the cooperation intent and personal objectives of the interacting vehicle i. The inner expectation then takes an average return of all plausible decisions by vehicle i conditioned on the parameters σ_i, w_i under our behavior model. The reward function \overline{Q}'_0 (·) represents the cumulative gain of the pairwise interaction between the ego vehicle and the vehicle i.

Based on the cumulative reward, the ego vehicle is controlled using a receding horizon control strategy, i.e.,

$$u_0^*(t) = \underset{u \in U}{\operatorname{argmax}} Q_0(s(t), u),$$
 (12)

where $Q_0(s(t),u)=\mathbb{E}_{\gamma_0\in\Gamma^1(u)}\left[Q_0'(s(t),\gamma_0)\right]$ and $\Gamma^1(u)$ contains all action sequences of length N with u being their initial action.

Remark. Note that the reward computation in Eq. (11) is not reactive. Our algorithm does not predict other vehicles' reactions to the ego actions in the prediction. To address this concern, we can also adopt a game-theoretic formulation similar to [12], [15]. However, such a formulation is computationally demanding in practice. Due to the formulation of pairwise interaction in Eq. (11), our algorithm can solve Eq. (12) effectively via an exhaustive search that scales linearly with the number of interacting vehicles.

V. SIMULATION AND EXPERIMENTAL RESULTS

Here, we demonstrate the effectiveness of the proposed behavioral model and the forced merging control algorithm. The behavioral model is first demonstrated by reproducing real-world driving behaviors. Then, the effectiveness of the proposed forced merging control algorithm is illustrated through simulation studies in comparison with the LFGC [12] against interacting vehicles controlled by our behavior model and through a naturalistic driving dataset [17].

A. Reproducing Real-world Traffic

We leverage a naturalistic traffic dataset called the High-D dataset [17]. It contains 60 traffic recordings among which three recordings/scenes (58-60) have merging ramps. We first calibrate the values of the model parameters a and $T_{\rm lane}$ from the High-D dataset (see Fig. 2). The lane width $w_{\rm lane}=3.5~{\rm m}$ in High-D. We choose $|a|=6~{\rm m/s^2}$ because the longitudinal accelerations and decelerations of High-D vehicles are within an interval of $[-6,6]~{\rm m/s^2}$. We select $T_{\rm lane}=4~{\rm sec}$ since the majority of the vehicles in the High-D dataset take $4\sim6~{\rm sec}$ to change lane.

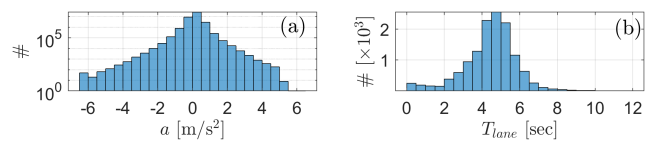


Fig. 2: Histogram of vehicle driving statistics in High-D dataset: (a) Longitudinal acceleration/deceleration (y-axis in log scale). (b) Time duration for a complete lane change.

We aim to reproduce the real-world driving behavior (see Fig. 3) in the recording segments using our behavioral model with certain parameters σ_i, w_i . Specifically, to reproduce the behavior of a target vehicle i, we initialize our behavioral model with its actual initial state $s_i(t=0)$ from the recording segment. At each time step of 2 seconds, we assume a virtual vehicle i is controlled by our behavior model, and can observe the surrounding traffic $s(t) = [s_i(t)^T, s_{A(i)}(t)^T]^T$. With prescribed parameters σ_i, w_i , the virtual vehicle i updates its control decision every time step using the behavioral model defined in Eq. (7) with MPC prediction horizon N=3spanning 6 seconds. The kinematics of the virtual vehicle obeys Eq. (1) with a sampling rate of 25 Hz. Furthermore, to introduce realistic lateral behaviors, the underlining lane change trajectories are modeled by 5th-order polynomials as proposed in [18].

As shown in Fig. 3a), the virtual truck 14 in green is controlled by our behavioral model with parameters $\sigma_{14} = \text{egoistic}$, $w_{14} = [0, 2/3, 1/3]^T$. This combination of parameters implies the virtual vehicle cares about the self-reward solely by the formulation in Eq. (3) and Eq. (5) and tries to minimize the traveling time because it has the largest weight 2/3 for τ in Eq. (4). As a result, the virtual truck merges into the highway, and the trajectory in the green boxes matches the actual target vehicle in the red boxes. As shown in Fig. 3b), in front of the virtual vehicle 13, there are two vehicles 12 and 15 driving slowly. With parameters

 $\sigma_{13}=$ competitive, $w_{14}=[0,1,0]^T$, the behavioral model controls the virtual vehicle to compete with the two vehicles while minimizing its traveling time. This interaction results in an overtaking behavior for the virtual vehicle which qualitatively matches the actual traffic recording. These examples provide evidence of our behavioral model being able to capture realistic driving behaviors. Note that there are quantitative mismatches in positions between the reproduced and the actual results in Fig. 3. Such mismatches partially result from the model assumption in Eq. (1); improvements to the kinematic model are left as future work.

B. Forced Merging in Simulation Compared with LFGC

We build up a highway with five vehicles (see Fig. 4) to simulate a forced merging scenario. The ego vehicle interacts with the surrounding traffic using the proposed controller in Eq. (12). In this example, each time step corresponds to one second and the lane change takes two time steps. Other vehicles are controlled using our behavioral model with different parameters σ_i, w_i . All the traffic vehicles are modeled as "egoistic" drivers, i.e., $\sigma_i =$ "egoistic" for all $i=1,\ldots,4$. We assign vehicle i=1,3,4 with weights $w_i=[0,0,1]$ to encourage minimization of control effort e such that the three vehicles will keep a constant speed. Vehicle 2 with weights $w_2=[1,0,0]$ tries to search for a larger headway space h, therefore, changes to the inner lane from t=0 to t=2 seconds.

We also deploy the LFGC to control the ego vehicle in the same highway traffic setting, and the results are plotted overlaid with ours in comparison (see Fig. 4). Note that the parameters σ_i and w_i of all vehicles 1-4 are not available to ego vehicle 0. As a result, the ego vehicle needs to interact with other vehicles and estimate their intentions online to facilitate its merging. During the simulation, our ego vehicle successfully infers the cooperative intents of vehicle 1,2,3 from their behaviors, and it decides to first accelerate to surpass vehicle 1 from t=0 to t=1, and merges into the gap created by the lane changing of vehicle 2.

We also provide our Bayesian filter estimation results (see Fig. 5) at time step t = 1. Here, we confine the domain of the weights w_i into a finite subset $W \subset [0,1]^3$ as follows

$$W = \left\{ \begin{bmatrix} [0,0,1], [0,1,1]/2, [0,1,0], [1,1,1]/3, \\ [1,0,1]/2, [1,1,0]/2, [1,0,0] \end{bmatrix}, (13) \right\}$$

where each weight case is a normalized combination of zeros and ones. Moreover, as shown in Fig. 5, the σ_i ="altruistic" category stands alone and is not correlated with the reward weights w_i because the "altruistic" driver does not care about the self-reward as modeled in Eqs. (3), (4) and (5). Notably, the actual parameters σ_i, w_i are among the ones of the highest probability. Meanwhile, for vehicle 2, the cases with the highest probability mostly emphasize traveling time τ and headway distance h while those of vehicles 1, 3 emphasize control effort e. Using these probability distributions, the ego vehicle can predict the driving and cooperation intent of vehicles 1, 2, 3, and plan its task accordingly, as demonstrated in Fig. 4.

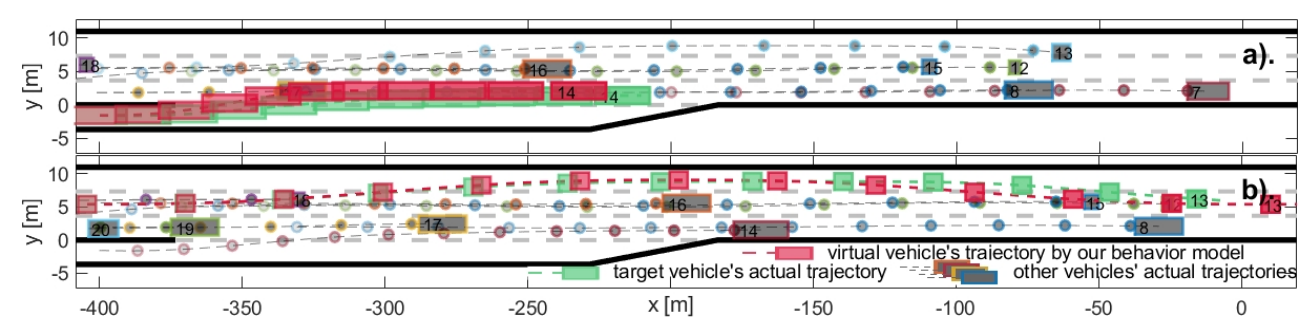


Fig. 3: Examples of reproducing real-world highway merging and overtaking behaviors: In each example, the target vehicle is represented by a green box, and interacts with the traffic. All traffic vehicles are visualized as boxes of different edge colors filled with grey. The trajectory of vehicles is shown in dashed lines with vehicles' positions every second marked as boxes in green (for the target vehicle) and circles filled with grey (for other traffic vehicles). The virtual vehicles' trajectories are visualized using red dashed lines and red boxes and match the actual ones closely. a) A traffic of 12 seconds is sampled from frames 1-300 in scene 59 from the High-D dataset. The trajectory of vehicle 14 is reproduced using our behavioral model with $\sigma_{14} = \text{egoistic}$, $w_{14} = [0, 2/3, 1/3]^T$, i.e., vehicle 14 is an egoistic driver, and minimizes the traveling time by merging to the highway. b) A traffic of 14 seconds is sampled from frames 1-350 in scene 59 from the High-D dataset. The trajectory of vehicle 13 is reproduced using our behavioral model with $\sigma_{13} = \text{competitive}$, $w_{13} = [0, 1, 0]^T$, i.e., vehicle 13 is a competitive driver, and minimizes the traveling time by overtaking the leading vehicles.

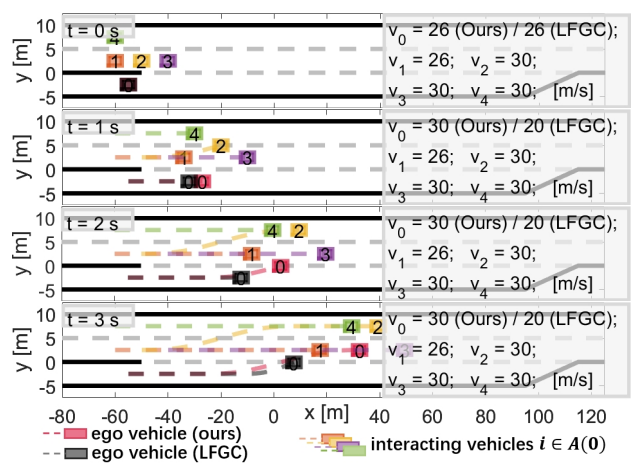


Fig. 4: Forced merging comparison in a simulation environment: Ego vehicle controlled by our algorithm in the red box interacts with the adjacent vehicles in colored boxes. The LFGC is tested using the same highway traffic setting, and the results are plotted overlaid using grey boxes. Four subfigures demonstrate the interactions at t=0,1,2,3 seconds, respectively. After accelerating to surpass vehicle 1, our ego vehicle properly merges into the highway at t=3 seconds.

In comparison, the ego vehicle controlled by the LFGC estimates the probability of the vehicle being a leader or being a follower, i.e., $\mathbb{P}\left(i=\text{``leader''}\right)=1-\mathbb{P}\left(i=\text{``follower''}\right), i=1,2,3,4$. However, due to the lane-changing behavior, the LFGC cannot distinguish between vehicle 2 being a "leader" and it being a "follower", namely, $\mathbb{P}\left(i=\text{``leader''}\right)=\mathbb{P}\left(i=\text{``follower''}\right)=0.5$. This results in a deceleration decision of the LFGC from t=0 to t=1. Seeing the constant-speed vehicle 1 as a "leader", the LFGC further keeps a low speed from t=1 to t=2 and decides to merge after vehicle 1 at t=2 while the ego vehicle controlled by our algorithm is in the middle of a lane change. This provides

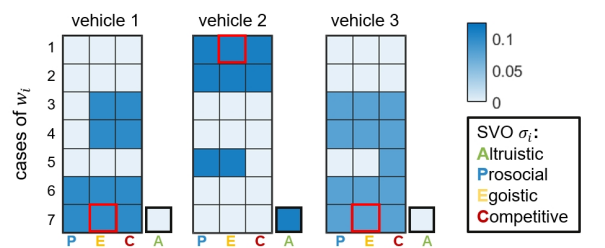


Fig. 5: Bayesian filter estimations of posterior $\mathbb{P}\left(\sigma_i,w_i|\xi(t)\right)$: Three sub-figures visualize the parameter belief of the interacting vehicles $i=1,\ 2,\ 3$, respectively, at t=1 second. The x axis labels the SVO categories σ_i , with the "altruistic" one standing alone. The y axis labels 7 different weights $w_i\in W$ with order listed in Eq. (13). The heatmap presents a higher probability with a deeper blue and the actual model parameters are circled in red.

evidence that, compared to the LFGC, our behavioral model captures a richer and more realistic set of behaviors and the controller integrated with our behavioral model can achieve faster merging in certain cases.

C. Validation on Real-world Dataset

To validate our controller in real-world traffic, we consider traffic segments (see Fig. 6) that contain merging vehicles from the High-D dataset. Similar to Sec. V-A, we use $w_{\rm lane}=3.5~{\rm m},~|a|=6~{\rm m/s^2},~T_{\rm lane}=4~{\rm sec},$ and an MPC prediction horizon N=3 spanning 6 seconds. We initialize our virtual ego vehicle using the initial state of the merging vehicle on the ramp. Afterward, we control the virtual ego vehicle with the proposed controller. We use the finite weight set W in Eq. (13) for parameter estimation in the Bayesian filter.

As shown in Fig. 6, the virtual ego vehicle interacts with two trucks 1 and 2 that drive approximately at constant speeds. Thus, the ego vehicle first accelerates to create

adequate merge space and speed advantage, then successfully merges between the two trucks. Notably, we can observe that the ego vehicle's trajectories are similar to the ones of the actual target vehicles, shown in green boxes.

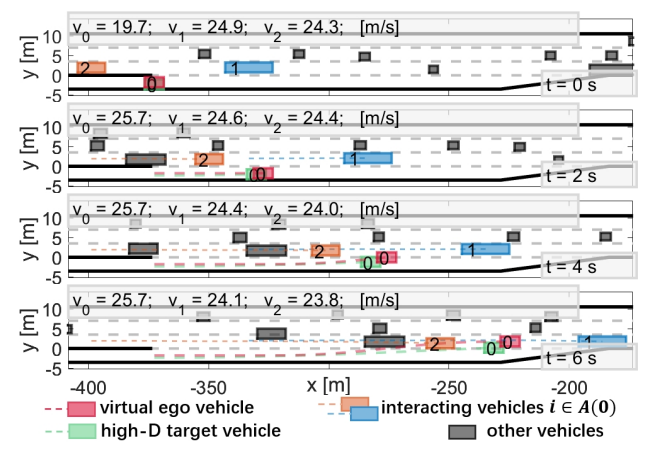


Fig. 6: Example of forced merging on the High-D dataset: the virtual ego vehicle in the red box is initialized using the target vehicle's initial state. Four rows demonstrate the interactions at t=0,2,4,6 seconds, respectively. After accelerating, the virtual ego vehicle properly merges onto the highway.

Meanwhile, in the High-D dataset, there are in total of 75 merging vehicles in scenes 58-60. For each merging vehicle, we repeat the aforementioned procedures to set up the test environment and control the virtual ego vehicle to merge onto the highway. The test results are presented in Table I. We consider a test case a success if the ego vehicle successfully merges without collisions. A failure case implies that the ego vehicle either collides with other vehicles or fails to merge by the end of the ramp. Our algorithm can achieve a 100% success rate among the 75 test cases, and properly merges the virtual vehicles into the naturalistic traffic.

TABLE I: High-D forced merging test results on scenes 58, 59, and 60: the traffic recordings in three scenes are recorded during different time intervals on Wednesday 07/2018 in the same highway location.

Scene Number	58	59	60	Total
Time Interval (AM)	9:15-9:22	9:23-9:31	9:37-9:53	
Number of Merges	18	21	36	75
Success	18	21	36	75
Failure	0	0	0	0
Success Rate (%)	100	100	100	100

VI. CONCLUSION

In this paper, we proposed a driving behavioral model that takes different social value orientations and personal objectives into consideration. Based on the proposed behavioral model, we developed a Bayesian filter that estimates online the latent cooperation intent of the interacting vehicles, and proposed a control algorithm that simultaneously achieves the merging objective and ensures driving safety. Finally,

we demonstrate the effectiveness of the proposed behavioral model and the forced merge control algorithm by reproducing real-world trajectories and evaluating the merging performance in simulations in comparison with the LFGC and a naturalistic traffic dataset.

REFERENCES

- M. Hügle, G. Kalweit, M. Werling, and J. Boedecker, "Dynamic interaction-aware scene understanding for reinforcement learning in autonomous driving," in *International Conference on Robotics and Automation (ICRA)*. IEEE, 2020, pp. 4329–4335.
- [2] Y. Pan, C.-A. Cheng, K. Saigol, K. Lee, X. Yan, E. Theodorou, and B. Boots, "Agile autonomous driving using end-to-end deep imitation learning," arXiv preprint arXiv:1709.07174, 2017.
- [3] B. R. Kiran, I. Sobh, V. Talpaert, P. Mannion, A. A. Al Sallab, S. Yo-gamani, and P. Pérez, "Deep reinforcement learning for autonomous driving: A survey," *Transactions on Intelligent Transportation Systems*, vol. 23, no. 6, pp. 4909–4926, 2021.
- [4] D. Sadigh, S. Sastry, S. A. Seshia, and A. D. Dragan, "Planning for autonomous cars that leverage effects on human actions." in *Robotics: Science and systems*, vol. 2. Ann Arbor, MI, USA, 2016, pp. 1–9.
- [5] C. You, J. Lu, D. Filev, and P. Tsiotras, "Advanced planning for autonomous vehicles using reinforcement learning and deep inverse reinforcement learning," *Robotics and Autonomous Systems*, vol. 114, pp. 1–18, 2019.
- [6] A. Gupta, J. Johnson, L. Fei-Fei, S. Savarese, and A. Alahi, "Social gan: Socially acceptable trajectories with generative adversarial networks," in *Conference on Computer Vision and Pattern Recognition* (CVPR), 2018, pp. 2255–2264.
- [7] S. Bae, D. Isele, A. Nakhaei, P. Xu, A. M. Añon, C. Choi, K. Fujimura, and S. Moura, "Lane-change in dense traffic with model predictive control and neural networks," *Transactions on Control Systems Technology*, 2022.
- [8] M. Liang, B. Yang, R. Hu, Y. Chen, R. Liao, S. Feng, and R. Urtasun, "Learning lane graph representations for motion forecasting," in *European Conference on Computer Vision (ECCV)*. Springer, 2020, pp. 541–556.
- [9] B. Ivanovic, K. Leung, E. Schmerling, and M. Pavone, "Multimodal deep generative models for trajectory prediction: A conditional variational autoencoder approach," *Robotics and Automation Letters*, vol. 6, no. 2, pp. 295–302, 2020.
- [10] N. Li, D. Oyler, M. Zhang, Y. Yildiz, A. Girard, and I. Kolmanovsky, "Hierarchical reasoning game theory based approach for evaluation and testing of autonomous vehicle control systems," in *Conference on Decision and Control (CDC)*. IEEE, 2016, pp. 727–733.
- [11] J. F. Fisac, E. Bronstein, E. Stefansson, D. Sadigh, S. S. Sastry, and A. D. Dragan, "Hierarchical game-theoretic planning for autonomous vehicles," in *International Conference on Robotics and Automation* (ICRA). IEEE, 2019, pp. 9590–9596.
- [12] K. Liu, N. Li, H. E. Tseng, I. Kolmanovsky, and A. Girard, "Interaction-aware trajectory prediction and planning for autonomous vehicles in forced merge scenarios," *Transactions on Intelligent Trans*portation Systems, 2022.
- [13] W. B. Liebrand, "The effect of social motives, communication and group size on behaviour in an n-person multi-stage mixed-motive game," *European Journal of Social Psychology*, vol. 14, no. 3, pp. 239–264, 1984.
- [14] D. M. Messick and C. G. McClintock, "Motivational bases of choice in experimental games," *Journal of Experimental Social Psychology*, vol. 4, no. 1, pp. 1–25, 1968.
- [15] W. Schwarting, A. Pierson, J. Alonso-Mora, S. Karaman, and D. Rus, "Social behavior for autonomous vehicles," *Proceedings of the National Academy of Sciences*, vol. 116, no. 50, pp. 24 972–24 978, 2019.
- [16] R. S. Sutton and A. G. Barto, Reinforcement learning: An introduction. MIT press, 2018.
- [17] R. Krajewski, J. Bock, L. Kloeker, and L. Eckstein, "The highd dataset: A drone dataset of naturalistic vehicle trajectories on german highways for validation of highly automated driving systems," in *International Conference on Intelligent Transportation Systems*. IEEE, 2018, pp. 2118–2125.
- [18] I. Papadimitriou and M. Tomizuka, "Fast lane changing computations using polynomials," in *Proceedings of the 2003 American Control Conference*, 2003., vol. 1. IEEE, 2003, pp. 48–53.